Topological Defects in Solids with Odd Elasticity

Lara Braverman, Colin Scheibner, Bryan VanSaders, and Vincenzo Vitelli

Phys. Rev. Lett. **127**, 268001 — Published 20 December 2021

DOI: 10.1103/PhysRevLett.127.268001

Topological defects in solids with odd elasticity

Lara Braverman,[1, 2, *] Colin Scheibner,[1, 2, *] Bryan VanSaders,[1, *] and Vincenzo Vitelli[1, 2, 3, †]

[1] *James Franck Institute, The University of Chicago, Chicago, Illinois 60637, USA*
[2] *Department of Physics, The University of Chicago, Chicago, Illinois 60637, USA*
[3] *Kadanoff Center for Theoretical Physics, The University of Chicago, Chicago, Illinois 60637, USA*

Crystallography typically studies collections of point particles whose forces are the gradient of an interaction potential. Lifting this assumption generically gives rise in the continuum limit to a form of elasticity with additional moduli known as odd elasticity. We show that such odd elastic moduli modify the strain induced by topological defects and their interactions, even reversing the stability of otherwise bound dislocation pairs. Beyond continuum theory, isolated dislocations can self propel via microscopic work cycles active at their cores that compete with conventional Peach-Koehler forces caused, for example, by an ambient torque density. We perform molecular dynamics simulations isolating active plastic processes and discuss their experimental relevance to solids composed of spinning particles, vortex-like objects, and robotic metamaterials.

Topological defects are local singularities in an order parameter that have global consequences at large scales [1–9]. In active systems, topological defects exhibit distinctive properties such as self-propulsion or nonreciprocal interactions [10–31]. In the study of crystalline defects, it is often assumed that a potential energy governs the interactions between the constituent particles. This assumption, however, need not hold in driven and active solids. For example, Fig. 1a shows a nonconservative interaction force—one in which the work done between any two configurations depends on the path taken. Such microscopic forces generically give rise in the continuum limit to odd elasticity: additional moduli that break the major symmetry of the elastic modulus tensor [32, 33]. Experimental signatures of odd elasticity have been reported in solids made of spinning embryos [34] and colloids [30] with hydrodynamic interactions, and robotic metamaterials [35, 36]. Likewise, gyroscopic matter [37–46] and vortex-like objects [47–55], e.g. skyrmions [56–61], can exhibit a special case of odd elastic dynamics (see S.I.).

Crystallography without potentials— A typical starting place in crystallography is a collection of point particles at positions $\underline{\mathbf{x}} = (\mathbf{x}^1, \mathbf{x}^2, \ldots, \mathbf{x}^N)$ interacting via forces that are the gradient of a potential:

$$\mathbf{F}^\alpha(\underline{\mathbf{x}}) = -\frac{\partial V(\underline{\mathbf{x}})}{\partial \mathbf{x}^\alpha} \tag{1}$$

However, in general, Eq. (1) need not be be valid. Experimentally relevant [29–31, 34, 62–67] counterexamples include pairwise forces of the form $\mathbf{F}^\alpha(\underline{\mathbf{x}}) = \sum_{\beta\neq\alpha} \mathbf{F}(\mathbf{x}^\alpha - \mathbf{x}^\beta)$ where $\mathbf{F}(\mathbf{r})$ depends only on particle separation:

$$\mathbf{F}(\mathbf{r}) = F^{\parallel}(r)\,\hat{\mathbf{r}} - F^{\perp}(r)\,\hat{\boldsymbol{\phi}} \tag{2}$$

Here, $\mathbf{r}$ is the relative coordinate between two interacting particles, $\hat{\boldsymbol{\phi}} = -\boldsymbol{\epsilon}\cdot\hat{\mathbf{r}}$, and $\boldsymbol{\epsilon}$ is the antisymmetric

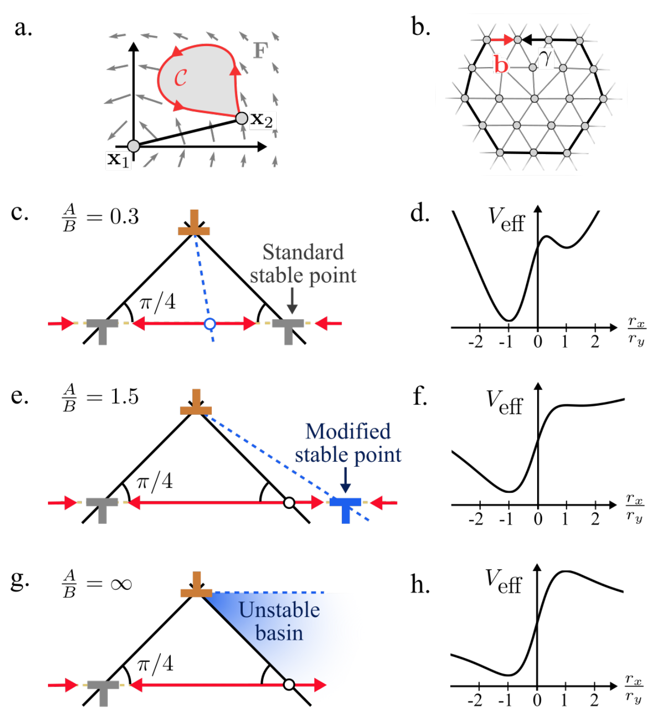

FIG. 1. **Odd elasticity modifies dislocation interactions and their stability. a.** A particle at point $\mathbf{x}_1$ exerts a force $\mathbf{F}$ on a particle at point $\mathbf{x}_2$. This force is nonconservative, so nonzero work is done along the closed cycle $\mathcal{C}$. **b.** A dislocation is defined by a Burgers vector $\mathbf{b}$ that represents the offset from what would otherwise be a closed loop γ. **c-d.** An orange dislocation is held stationary while a second anti-aligned dislocation is free to move along its glide plane subject to the Peach-Koehler force (red arrows). When $|A/B| < 1$, the free dislocation has two stable points located along rays forming an angle $\pi/4$ with the glide plane. The effective potential $V_{\rm eff}$ as a function of the horizontal (r_x) and vertical (r_y) distance between the dislocations. **e-f.** When $A/B > 1$, the rightmost stable equilibrium moves outward beyond $\pi/4$. **g-h**. When $A/B = \infty$, only one stable equilibrium position exists and the shaded region is an unstable basin.

* These authors contributed equally to this work.
† vitelli@uchicago.edu

tensor. We will henceforth focus on first order dynamics $\dot{\mathbf{x}}^\alpha = \mathbf{F}^\alpha$, which arise in overdamped media, as well as in vortex [47–55] and gyroscopic [37–46] crystals in which the forces $\mathbf{F}^\alpha = \boldsymbol{\epsilon} \cdot \frac{\partial V}{\partial \mathbf{x}^\alpha}$ are transverse to potential gradients, see S.I.§S1A. Subject to first order dynamics, the quantity $P \equiv \dot{\mathbf{x}}^\alpha \cdot \mathbf{F}^\alpha(\underline{\mathbf{x}})$ is greater than zero for trajectories satisfying the equations of motion [68]. Of particular interest here are interparticle forces such that $W_\gamma = \oint_\gamma P \, \mathrm{d}t \neq 0$ for closed contours γ (see Fig. 1a). Notice that $\nabla \times \mathbf{F} = 0$ is equivalent to requiring that $W_\gamma = 0$ for all contractible loops γ. In Newtonian mechanics, W_γ has the interpretation of energy, and $\nabla \times \mathbf{F} \neq 0$ is equivalent to violating Maxwell-Betti reciprocity (MBR) [69], which means that the linear response matrix between force and displacement is no longer symmetric, see S.I.§S1A.

Continuum theory— In the continuum, we describe the state of the solid via a continuous displacement field $\mathbf{u}(\mathbf{r})$ and we assume that the coarse-grained forces may be expressed as $f_j = \partial_i \sigma_{ij}$, where σ_{ij} is the Cauchy stress tensor (see Ref. [28] for a treatment of dislocations that lifts this assumption). We expand the Cauchy stress tensor σ_{ij} in terms of the displacement gradient u_{mn} to obtain $\sigma_{ij} = \sigma^0_{ij} + C_{ijmn} u_{mn}$. Here, C_{ijmn} denotes the elastic modulus tensor and σ^0_{ij} is the stress prior to deformation. In 2D isotropic crystals, the linearized stress-strain relationship is summarized by the pictorial equation [32]:

$$\begin{pmatrix} \cdot \\ \cdot \\ \cdot \\ \cdot \end{pmatrix} = \begin{pmatrix} -p_0 \\ -\tau_0 \\ 0 \\ 0 \end{pmatrix} + \begin{pmatrix} B & \Lambda & 0 & 0 \\ A & \Gamma & 0 & 0 \\ 0 & 0 & \mu & K^o \\ 0 & 0 & -K^o & \mu \end{pmatrix} \begin{pmatrix} \cdot \\ \cdot \\ \cdot \\ \cdot \end{pmatrix} \quad (3)$$

See S.I.§S1C for tensor notation. In Eq. (3), p_0 and τ_0 are mechanically interpreted in terms of the pressure and torque density associated with σ^0_{ij}. The matrix in Eq. (3) corresponds to C_{ijmn} and has three diagonal components, the bulk B, shear μ, and rotational Γ moduli, and three off-diagonal moduli Λ, A, and K^o. The antisymmetric contributions to the matrix in Eq. (3) are what we refer to as *odd elastic moduli* [32]. The counterpart of $P = \dot{\mathbf{x}}^\alpha \cdot \mathbf{F}^\alpha$ in the continuum is $P = \int S_{ij} \dot{u}_{ij} \mathrm{d}^2 r$, where S_{ij} is the first Piola-Kirchoff tensor [70–74]. Writing $S_{ij} = S^0_{ij} + \tilde{C}_{ijmn} u_{mn}$, we have

$$\tilde{C}_{mnij} = C_{ijmn} + \sigma^0_{ij}\delta_{mn} - \sigma^0_{mj}\delta_{in} \quad (4)$$

In the continuum, the Maxwell-Betti reciprocity theorem states the internal forces must be non-conservative if $\tilde{C}_{ijmn} \neq \tilde{C}_{mnij}$ [69]. Odd elasticity ($C_{ijkl} \neq C_{klij}$) coincides with broken MBR ($\tilde{C}_{ijkl} \neq \tilde{C}_{klij}$) when no ambient stress is present ($\sigma^0_{ij} = 0$). In terms of the moduli in Eq. (3) the condition for MBR, $\tilde{C}_{ijmn} = \tilde{C}_{mnij}$, reads:

$$2K^o = \Lambda - A = 2\tau_0 \quad (5)$$

Notice from Eq. (5) that odd elasticity can arise even when MBR holds (i.e. the microscopic forces are conservative) provided that τ_0 is nonvanishing. For instance,

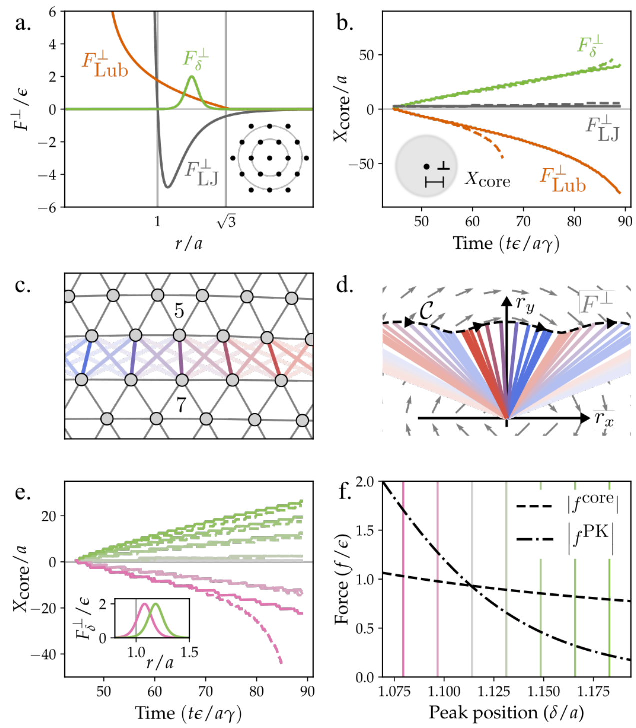

FIG. 2. **Dislocations self propel via active work cycles at their cores.** **a.** Three transverse interactions $F^\perp_{\mathrm{LJ}}$ (purple), $F^\perp_{\mathrm{Lub}}$ (teal), and $F^\perp_\delta$ (orange), with the neighbor shells highlighted by grey lines. Inset: A hexagonal lattice with first and second neighbor shells highlighted. **b.** Particles are arranged in a free floating circular cluster with a single dislocation located at the center, and the dislocation position is tracked as function of time. Simulation are performed with clusters of radius $R = 50$ (dashed) and $R = 100$ (solid). See Supplemental Movie S1. **c.** Bonds crossing the glide plane of a dislocation are highlighted. Hue indicates the bond's position in real space (blue: left, red: right). Opacity indicates the length of the bond (nearest neighbors darkest). **d.** The highlighted bonds are plotted with their bases aligned. As the dislocation moves one unit cell to the right, the tops of the bonds traces out a contour $\mathcal{C}$ (black dashed). The gray arrows depict the interaction force field. See Supplemental Movie S2. **e.** The interaction $F^\perp_\delta$ is varied by changing the location δ of its peak (pink: smaller δ, green: larger δ). For each value of δ, the dislocation's position is tracked as a function of time. **f.** The magnitude of the Peach-Koehler force f^{PK} and the active core force f^{core} as a function of the peak position δ. The vertical lines represent the values of δ used in the simulation. The direction change of the dislocation motion coincides with the crossover between f^{core} and f^{PK}.

the transverse microscopic force $F^\perp(r) \propto \frac{1}{r}$ is curl-free, i.e. conservative, and nonetheless gives rise to A and K^o (S.I.§S1E). In this case A and K^o can be detected from static stress-strain measurements, but the work they generate during strain cycles must be cancelled by τ_0. The distinction between C_{ijkl} and $\tilde{C}_{ijkl}$ vanishes when no ambient stress σ^0_{ij} is present. See §S1E for how crystals with purely transverse interactions, such as lattices of vortex-like objects [47–61] or gyroscopes [37–46], can be mathematically cast as a special case of odd elasticity with $B = \mu = 0$.

Microscopics—To relate the moduli to the microscopic transverse forces, we linearize Eq. (2) about the lattice spacing a: $F^{\perp}(r) = F_0^{\perp} - k^a(r-a)$. The resulting odd elastic moduli for an hexagonal lattice read

$$A \approx \frac{\sqrt{3}}{2}\left(k^a + \frac{F_0^{\perp}}{a}\right) \quad K^o \approx \frac{\sqrt{3}}{4}\left(k^a - \frac{3F_0^{\perp}}{a}\right) \tag{6}$$

along with an ambient torque density $\tau_0 = \sqrt{3}F_0^{\perp}/a$, see S.I.§S1D and Refs. [28, 32]. Additionally, the modulus A arises whenever the full torque density $\tau = \epsilon_{ij}\sigma_{ij}/2$ couples to local dilation $\partial_i u_i = -\delta\rho/\rho_0$, namely $A = \frac{\mathrm{d}\tau}{\mathrm{d}\rho}\rho_0$. The forces in Eq. (2) depend only on r, and therefore cannot contribute to Γ and Λ which couple to solid body rotations. However, Γ and Λ can arise in response to external fields or interactions with a substrate [8], see S.I.§S1E for examples. We henceforth set $\Lambda = \Gamma = 0$, see S.I.§S2C for a general treatment [75].

Continuum solutions— Topological defects are singularities where $u_i(\mathbf{r})$ becomes multi-valued, e.g. the dislocation in Fig. 1b is defined by the Burgers vector b_i

$$b_j = \oint_{\gamma} \partial_i u_j \mathrm{d}r_i \tag{7}$$

where γ is a counterclockwise contour around the dislocation. We solve $\partial_i\sigma_{ij}(\mathbf{r}) = 0$ together with Eq. (7) to obtain static solutions of the dislocation displacement field (S.I.§S2C):

$$\mathbf{u}_{\mathrm{disl}} = \frac{1}{2\pi}\Big\{\phi\,\mathbf{b} + \frac{1-\nu}{2}\log(r)\,\boldsymbol{\epsilon}\cdot\mathbf{b} - \frac{1+\nu}{2}(\hat{\mathbf{r}}\cdot\mathbf{b})\,\hat{\boldsymbol{\phi}} - \nu^o\Big[\log(r)\,\mathbf{b} + (\hat{\boldsymbol{\phi}}\cdot\mathbf{b})\,\hat{\boldsymbol{\phi}}\Big]\Big\} \tag{8}$$

where r and ϕ are polar coordinates about the defect. The elastic properties enter only through (i) a modified Poisson's ratio, ν, (S.I.§S2C) and (ii) a purely nonreciprocal *odd ratio* [32]

$$\nu^o = \frac{BK^o - A\mu}{\mu(B+\mu) + K^o(A+K^o)} \tag{9}$$

The effect of ν^o in Eq. (8) is to globally rotate the local shear axis by an angle $\delta\alpha$

$$\delta\alpha = -\frac{1}{2}\arctan\left(\frac{2\nu^o}{1+\nu}\right) \tag{10}$$

See Fig. S5-6 for an illustration and numerical validation. S.I.§S2B provides similar results for point defects and isolated disclinations, which have recently been observed in experiments [34] of spinning embryos interacting via transverse forces, cf. Eq. (2).

Dislocation interactions— The modified stress field alters dislocation interactions. Consider first the work done in quasistatically moving a test dislocation by δX_i through a pre-existing stress field $\sigma_{ij}^{(\mathrm{pre})}$ obeying $\partial_i\sigma_{ij}^{(\mathrm{pre})} = 0$. Regardless of the material's constitutive properties, the work done by $\sigma_{ij}^{(\mathrm{pre})}$ is given by the Peach-Koehler (PK) formula $\delta W = f_m^{\mathrm{PK}}\delta X_m$, where $f_m^{\mathrm{PK}} = \epsilon_{mi}\sigma_{ij}^{(\mathrm{pre})}b_j$ (S.I.§S3A). The continuum interaction between two dislocations is the PK force experienced by the test dislocation as a result of the stress field generated by the other. In Fig. 1c-h, we examine the interaction between two antiparallel dislocations in the presence of odd elastic moduli. The modulus A provides a nontrivial modification:

$$f^{\mathrm{PK}}(r_x) = \frac{(1-\nu)b_1b_2}{\pi r^4}(r_x^2 - r_y^2)(Br_x + Ar_y) \tag{11}$$

where f^{PK} is the PK force projected onto the glide plane of the dislocation. When $A = 0$, the dislocations obey the classic result: their separation vector forms an angle $\pi/4$ with respect to their glide planes [2, 76]. When $0 < A/B < 1$, the mechanically stable positions remain the same while their basins of attraction change. When $A/B > 1$, the right equilibrium point moves out beyond the $\pi/4$ angle. When $A/B \to \infty$, the rightmost basin becomes unstable. When the Burgers vectors are not parallel, the dislocation interactions are non-reciprocal in the sense of being non-mutual: their forces are not equal and opposite (S.I.§S3B).

Dislocation motion from PK forces— While the continuum theory provides insights at long lengths scales, whether and in what directions dislocations actually move depends on microscopic details. To illustrate this, we perform overdamped molecular dynamics simulations of particles interacting with a radial force $F^{\parallel}(r)$ given by a Lennard-Jones (LJ) force and three different realizations of the transverse force $F^{\perp}(r)$ in Eq. (2), see Fig. 2a-b and Movie S1.

Consider first a transverse interaction $F_{\mathrm{LJ}}^{\perp}(r)$, which like $F^{\parallel}$, is an LJ force: a dislocation introduced to the center remains stationary as in a passive crystal. The reason is that the total force on any particle is simply a rotation of the force due to $F^{\parallel}$. Hence the static configuration guaranteed by energy minimization for $F^{\parallel}$ remains static when $F_{\mathrm{LJ}}^{\perp}$ is introduced. Next we introduce $F_{\mathrm{Lub}}^{\perp}$, which is a monotonically decreasing function of a single sign shown in Fig. 2a, generically representative of hydrodynamic, lubrication and frictional forces between self-spinning particles [29, 34, 62, 66, 67]. For $F_{\mathrm{Lub}}^{\perp}$, the dislocation travels at a near constant speed to the left. Since $F_{\mathrm{Lub}}^{\perp}$ is nonzero at the first neighbor shell, it produces an ambient torque density τ_0. Upon setting $\sigma_{ij}^{(\mathrm{pre})} = \tau_0\epsilon_{ij}$, the direction of dislocation motion follows the standard PK force expression $f_i^{\mathrm{PK}} = \epsilon_{ij}\sigma_{jk}^{(\mathrm{pre})}b_k = -\tau_0 b_i$, in agreement with the experiments and analysis of spinning-colloids crystals in Refs. [28, 30].

Dislocation self-propulsion from microscopic work cycles at their cores— We now show that not all mechanisms of dislocation propulsion can be captured by con-

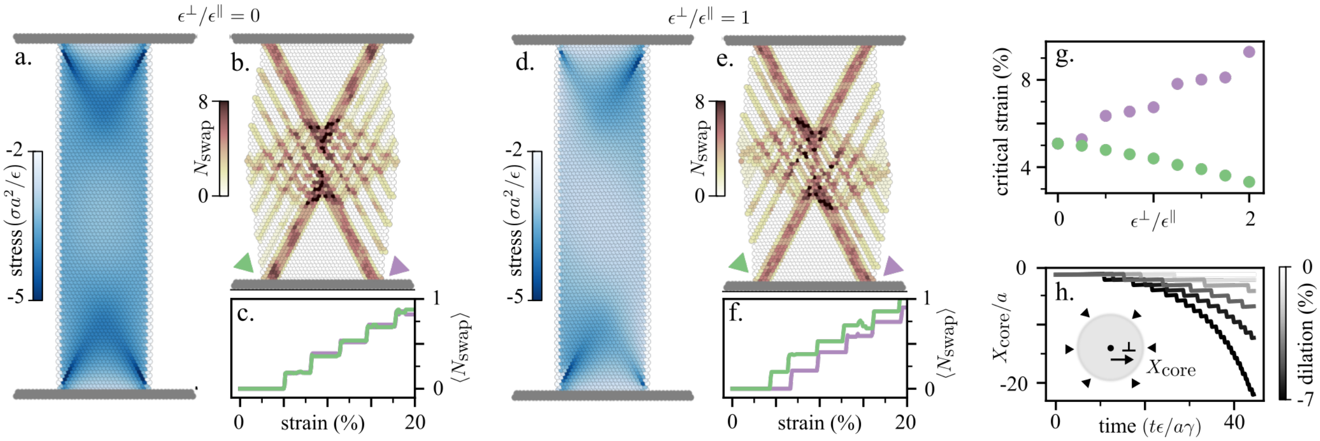

FIG. 3. **Active plasticity in odd elastic media. a-c.** The compression of a solid beam with a standard LJ interactions of strength $\epsilon^\parallel$. **d-f.** The same numerical experiment with the addition of transverse lubrication forces of magnitude $\epsilon^\perp$. See Supplemental Movies S3-4. (a., d.) show the per-particle stress, resolved on the [11] and [$\bar{1}$1] glide planes and summed, immediately prior to the first dislocation nucleation. (b., e.) After significant plastic deformation, we color particles by the cumulative number of neighbor changes in their first coordination shell ($N_{\rm swap}$). (c., f.) $N_{\rm swap}$ averaged in the vicinity of the lower-left- and lower-right-hand corners as a function of strain. The strain is $\Delta h/h$ where h is the height of the beam. **g.** The critical strain at first nucleation for the bottom left-hand (green) and right-hand (pink) corners. **h.** A disk of particles interacting via radial and transverse LJ forces is subject to compression (negative dilation). At higher compression, a torque density is induced throughout the cluster which drives dislocation motion via the PK force. See the S.I.§S5 for additional simulation details.

tinuum considerations. The continuum PK force is derived from a coarsegrained approximation to the work done during dislocation motion. However, when a potential is not well defined, contributions to δW from short lengthscales need not average out during dislocation motion. In some cases, they can even overcome continuum predictions. To illustrate this, we use as a probe the force $F_\delta^\perp(r)$ narrowly peaked at a tunable interparticle distance $r=\delta$ and with same sign as $F_{\rm Lub}^\perp$. However, when the peak δ lies half way between the first and second neighbor shells, the dislocation now travels to the right, the opposite direction of $F_{\rm Lub}^\perp$ (see Fig. 2ab). Since the force $F_\delta^\perp$ is negligible at the first and second neighbor shells, the odd moduli A and K^o as well as the ambient torque density τ_0 are vanishingly small. This suggests that the underlying mechanism of dislocation motility evades the standard continuum explanation in term of PK forces provided in the previous paragraph.

As we now show, this dislocation motility is a form of self-propulsion associated with microscopic work cycles acting at dislocation cores. We first highlight all the bonds that straddle the glide plane (Fig. 2c) and align their bases so that they are viewed in the space of their relative coordinates (r_x, r_y) (Fig. 2d). Crucially, as the dislocation moves by a single unit cell, each highlighted bond assumes the position of its neighbor to the right. Next, we concatenate all the individual bond trajectories into a single contour $\mathcal{C}$ (dashed line) that begins at $r_x=-\infty$ and ends at $r_x=\infty$. The total work done when each of the bonds moves a short distance is then equivalent to that of a single bond traveling the entire contour, c.f. Fig. 1a. Notice that if the force falls off faster than $1/r$, then the contour may be closed in the upper half plane. Similar to the single-bond cycle shown in Fig. 1a, the corresponding work $W_{\rm glide}$ reads

$$W_{\rm glide} \approx \oint_{\mathcal{C}} \mathbf{F}\cdot \mathrm{d}\mathbf{r} = \int_{\mathcal{A}} \nabla\times\mathbf{F}\,\mathrm{d}^2 r \tag{12}$$

where $\mathcal{A}$ is the upper half plane enclosed by $\mathcal{C}$ (S.I.§S4 and Movie S2).

Since $W_{\rm glide}$ is associated with motion through one lattice spacing, the corresponding force on the dislocation reads $f^{\rm core}=\frac{1}{a}W_{\rm glide}$ and it is directed along the glide plane. In principle, the detailed shape of $\mathcal{C}$ depends on protocol and dynamics. However, a useful first approximation is to take $\mathcal{C}$ to be the line at $r_y=\frac{\sqrt{3}}{2}a$, giving:

$$f^{\rm core} = \frac{1}{a}W_{\rm glide} \approx \frac{1}{a}\int_{-\infty}^{\infty} F_x^\perp \mathrm{d}r_x\Big|_{r_y=\frac{\sqrt{3}}{2}a} \tag{13}$$

In Fig. 2e we perform simulations with $F_\delta^\perp$ but we vary the parameter δ, which sets the location of the central peak. At small δ, there is significant overlap between $F_\delta^\perp$ and the first neighbor shell, giving rise to a large ambient torque density $\tau_0\approx\sqrt{3}F^\perp(a)/a$ and corresponding PK force $f^{\rm PK}$. Fig. 2f shows the relative magnitudes of $f^{\rm core}$ and $f^{\rm PK}$ as a function of δ. The crossover in dominant force coincides with the sign reversal in dislocation speed corroborating our theoretical derivation of $f^{\rm core}$. While the sign-reversal is a dramatic effect that occurs under specific conditions, $f^{\rm core}$ is generically present for all non-conservative microscopic interaction forces. Solids whose microscopic interactions violate Newton's third law can also display spontaneous dislocation motion [28].

Active plasticity— Finally, we examine the effects of odd elasticity on plastic deformation. In Fig. 3a, we perform a simple uniaxial compression of a solid interacting via a transverse lubrication force (see also Supplemental Movies S3-4). Before the first dislocation nucleates, odd elasticity biases the stress distribution (Fig. 3a,d). At the end of the compression, the permanently deformed shape of the beam breaks all mirror symmetries (Fig. 3b,e). The change in final shape arises because the biased stress distribution favors dislocation nucleation from the upper-right- and lower-left-hand corners (Fig. 3c,f). Empirically, we find that introducing transverse forces generally lowers the plastic yield strain at which the first dislocation nucleates (Fig. 3g). In Fig. 3h, we consider a single dislocation in the center of a disk. In a passive medium, a uniform compression induces an isotropic stress $-B(\delta\rho/\rho)\delta_{ij}$ with an associated $f_i^{\mathrm{PK}} = -B(\delta\rho/\rho)\epsilon_{ij}b_j$ in the climb direction. This typically results in no motion or defect splitting. The odd elastic solid in Fig. 3h features a $F_{\mathrm{LJ}}^{\perp}$ which induces no dislocation motion in the absence of external stresses (recall Fig. 2b). However, due to the odd modulus A, an area change gives rise to a torque density $\tau = A(\delta\rho/\rho)$, which in turn promotes motion along the glide plane via $f_i^{\mathrm{PK}} = -\tau b_i$.

To summarize, we studied how defect strains, interactions and motility are modified in systems for which the interactions are more general than standard pairwise, potential forces.

ACKNOWLEDGMENTS

V.V. acknowledges support from the Simons Foundation, the Complex Dynamics and Systems Program of the Army Research Office under grant W911NF-19-1-0268, and the University of Chicago Materials Research Science and Engineering Center, which is funded by the National Science Foundation under Award No. DMR-2011854. C.S. acknowledges support from the Bloomenthal Fellowship and the National Science Foundation Graduate Research Fellowship under Grant No. 1746045. L.B. acknowledges support from the Heising-Simons Scholarship and the James Franck Institute Undergraduate Summer Research Award. B.V.S acknowledges support from the Kadanoff-Rice Postdoctoral Fellowship. Some of us benefited from participation in the KITP program on Symmetry, Thermodynamics and Topology in Active Matter supported by Grant No. NSF PHY-1748958. This work was completed in part with resources provided by the University of Chicago Research Computing Center. The authors would like to thank M. Han, M. Fruchart, A. Poncet, D. Bartolo and W. Irvine for helpful conversations.

[1] Nelson, D. R. *Defects and geometry in condensed matter physics* (Cambridge University Press, Cambridge ; New York, 2002).

[2] Weertman, J. *Elementary dislocation theory.* Macmillan series in materials science (Macmillan, New York, 1964).

[3] Chaikin, P. M. *Principles of condensed matter physics* (Cambridge University Press, Cambridge ; New York, NY, USA, 1995).

[4] Paulose, J., Chen, B. G.-g. & Vitelli, V. Topological modes bound to dislocations in mechanical metamaterials. *Nat Phys* **11**, 153–156 (2015).

[5] Mietke, A. & Dunkel, J. Anyonic defect braiding and spontaneous chiral symmetry breaking in dihedral liquid crystals. *arXiv:2011.04648* (2020).

[6] Pretko, M. & Radzihovsky, L. Fracton-elasticity duality. *Phys. Rev. Lett.* **120**, 195301 (2018).

[7] Bowick, M. J. & Giomi, L. Two-dimensional matter: order, curvature and defects. *Advances in Physics* **58**, 449–563 (2009).

[8] Nelson, D. & Halperin, B. Dislocation-mediated melting in two dimensions. *Phys. Rev. B* **19**, 2457–2484 (1979).

[9] Wachtel, G., Sieberer, L. M., Diehl, S. & Altman, E. Electrodynamic duality and vortex unbinding in driven-dissipative condensates. *Phys. Rev. B* **94**, 104520 (2016).

[10] Shankar, S., Souslov, A., Bowick, M. J., Marchetti, M. C. & Vitelli, V. Topological active matter. *arXiv:2010.00364* (2020).

[11] Giomi, L., Hawley-Weld, N. & Mahadevan, L. Swarming, swirling and stasis in sequestered bristle-bots. In *Proceedings of the Royal Society of London A: Mathematical, Physical and Engineering Sciences*, vol. 469, 20120637 (The Royal Society, 2013).

[12] Duclos, G. *et al.* Topological structure and dynamics of three-dimensional active nematics. *Science* **367**, 1120–1124 (2020).

[13] Colen, J. *et al.* Machine learning active-nematic hydrodynamics. *Proceedings of the National Academy of Sciences* **118** (2021).

[14] Vafa, F., Bowick, M. J., Marchetti, M. C. & Shraiman, B. I. Multi-defect dynamics in active nematics. *arXiv:2007.02947* (2020).

[15] Pearce, D. J. G., Gat, S., Livne, G., Bernheim-Groswasser, A. & Kruse, K. Programming active metamaterials using topological defects. *arXiv:2010.13141* (2020).

[16] Thijssen, K. & Doostmohammadi, A. Binding self-propelled topological defects in active turbulence. *Phys. Rev. Research* **2**, 042008 (2020).

[17] Rouzaire, Y. & Levis, D. Defects superdiffusion and unbinding in a 2d xy model of self-driven rotors. *arXiv:2103.12578* (2021).

[18] Chardac, A., Hoffmann, L. A., Poupart, Y., Giomi, L. & Bartolo, D. Topology-driven ordering of flocking matter (2021). 2103.03861.

[19] Fruchart, M., Hanai, R., Littlewood, P. B. & Vitelli, V. Non-reciprocal phase transitions. *Nature* **592**, 363–369 (2021).

[20] Whitfield, C. A. *et al.* Hydrodynamic instabilities in ac-

tive cholesteric liquid crystals. *The European Physical Journal E* **40**, 50 (2017).

[21] Kole, S. J., Alexander, G. P., Ramaswamy, S. & Maitra, A. Layered chiral active matter: Beyond odd elasticity. *Phys. Rev. Lett.* **126**, 248001 (2021).

[22] Maitra, A., Lenz, M. & Voituriez, R. Chiral active hexatics: Giant number fluctuations, waves, and destruction of order. *Phys. Rev. Lett.* **125**, 238005 (2020).

[23] Gupta, R. K., Kant, R., Soni, H., Sood, A. K. & Ramaswamy, S. Active nonreciprocal attraction between motile particles in an elastic medium. *arXiv:2007.04860* (2020).

[24] Kumar, N., Soni, H., Ramaswamy, S. & Sood, A. K. Flocking at a distance in active granular matter. *Nature Communications* **5**, 4688 (2014).

[25] VanSaders, B. & Glotzer, S. C. Designing active particles for colloidal microstructure manipulation via strain field alchemy. *Soft Matter* **15**, 6086–6096 (2019).

[26] VanSaders, B. & Glotzer, S. C. Sculpting crystals one burgers vector at a time: Toward colloidal lattice robot swarms. *Proceedings of the National Academy of Sciences* **118** (2021).

[27] Digregorio, P., Levis, D., Cugliandolo, L. F., Gonnella, G. & Pagonabarraga, I. Unified analysis of topological defects in 2d systems of active and passive disks. *arXiv:2106.03454* (2021).

[28] Poncet, A. & Bartolo, D. When soft crystals defy newton's third law: Non-reciprocal mechanics and dislocation motility (2021). 2110.02897.

[29] Yan, J., Bae, S. C. & Granick, S. Rotating crystals of magnetic Janus colloids. *Soft Matter* **11**, 147–153 (2015).

[30] Bililign, E. S. *et al.* Chiral crystals self-knead into whorls. *arXiv:2102.03263* (2021).

[31] van Zuiden, B. C., Paulose, J., Irvine, W. T. M., Bartolo, D. & Vitelli, V. Spatiotemporal order and emergent edge currents in active spinner materials. *Proc. Natl. Acad. Sci. USA* **113**, 12919–12924 (2016).

[32] Scheibner, C. *et al.* Odd elasticity. *Nature Physics* **16**, 475–480 (2020).

[33] Scheibner, C., Irvine, W. T. M. & Vitelli, V. Non-hermitian band topology and skin modes in active elastic media. *Phys. Rev. Lett.* **125**, 118001 (2020).

[34] Tan, T. H. *et al.* Development drives dynamics of living chiral crystals. *arXiv:2105.07507* (2021).

[35] Chen, Y., Li, X., Scheibner, C., Vitelli, V. & Huang, G. Realization of active metamaterials with odd micropolar elasticity. *Nature Communications* **12**, 5935 (2021).

[36] Brandenbourger, M., Scheibner, C., Veenstra, J., Vitelli, V. & Coulais, C. Active impact and locomotion in robotic matter with nonlinear work cycles. *arXiv:2108.08837* (2021).

[37] Wang, P., Lu, L. & Bertoldi, K. Topological Phononic Crystals with One-Way Elastic Edge Waves. *Physical review letters* **115**, 104302 (2015).

[38] Zhao, Y., Zhou, X. & Huang, G. Non-reciprocal rayleigh waves in elastic gyroscopic medium. *Journal of the Mechanics and Physics of Solids* **143**, 104065 (2020).

[39] Carta, G., Brun, M., Movchan, A., Movchan, N. & Jones, I. Dispersion properties of vortex-type monatomic lattices. *International Journal of Solids and Structures* **51**, 2213 – 2225 (2014).

[40] Hassanpour, S. Dynamics of gyroelastic continua (2014).

[41] Carta, G., Jones, I. S., Movchan, N. V., Movchan, A. B. & Nieves, M. J. "deflecting elastic prism"and unidirectional localisation for waves in chiral elastic systems. *Scientific Reports* **7**, 26 (2017).

[42] Nash, L. M. *et al.* Topological mechanics of gyroscopic metamaterials. *Proc. Natl. Acad. Sci. USA* **112**, 14495–500 (2015).

[43] Mitchell, N. P., Nash, L. M. & Irvine, W. T. M. Tunable band topology in gyroscopic lattices. *Phys. Rev. B* **98**, 174301 (2018).

[44] Mitchell, N. P., Nash, L. M. & Irvine, W. T. M. Realization of a topological phase transition in a gyroscopic lattice. *Phys. Rev. B* **97**, 100302 (2018).

[45] Mitchell, N. P., Nash, L. M., Hexner, D., Turner, A. M. & Irvine, W. T. M. Amorphous topological insulators constructed from random point sets. *Nature Physics* **14**, 380–385 (2018).

[46] Brun, M., Jones, I. S. & Movchan, A. B. Vortex-type elastic structured media and dynamic shielding. *Proceedings of the Royal Society A: Mathematical, Physical and Engineering Sciences* **468**, 3027–3046 (2012).

[47] Sonin, E. B. Vortex oscillations and hydrodynamics of rotating superfluids. *Rev. Mod. Phys.* **59**, 87–155 (1987).

[48] Gifford, S. A. & Baym, G. Dislocation-mediated melting in superfluid vortex lattices. *Phys. Rev. A* **78**, 043607 (2008).

[49] Nguyen, D. X., Gromov, A. & Moroz, S. Fracton-elasticity duality of two-dimensional superfluid vortex crystals: defect interactions and quantum melting. *arXiv:2005.12317* (2020).

[50] Moroz, S., Hoyos, C., Benzoni, C. & Son, D. T. Effective field theory of a vortex lattice in a bosonic superfluid. *SciPost Phys.* **5**, 39 (2018).

[51] Fetter, A. L. Rotating trapped bose-einstein condensates. *Rev. Mod. Phys.* **81**, 647–691 (2009).

[52] Blatter, G., Feigel'man, M. V., Geshkenbein, V. B., Larkin, A. I. & Vinokur, V. M. Vortices in high-temperature superconductors. *Rev. Mod. Phys.* **66**, 1125–1388 (1994).

[53] Tkachenko, V. K. Elasticity of vortex lattices. *JETP* **29**, 945 (1969).

[54] Tkachenko, V. On vortex lattices. *Sov. Phys. JETP* **22**, 1282–1286 (1966).

[55] Tkachenko, V. Stability of vortex lattices. *Sov. Phys. JETP* **23**, 1049–1056 (1966).

[56] Benzoni, C., Jeevanesan, B. & Moroz, S. Rayleigh edge waves in two-dimensional crystals with lorentz forces: From skyrmion crystals to gyroscopic media. *Phys. Rev. B* **104**, 024435 (2021).

[57] Huang, P. *et al.* Melting of a skyrmion lattice to a skyrmion liquid via a hexatic phase. *Nature Nanotechnology* **15**, 761–767 (2020).

[58] Ochoa, H., Kim, S. K., Tchernyshyov, O. & Tserkovnyak, Y. Gyrotropic elastic response of skyrmion crystals to current-induced tensions. *Phys. Rev. B* **96**, 020410 (2017).

[59] Mühlbauer, S. *et al.* Skyrmion lattice in a chiral magnet. *Science* **323**, 915–919 (2009).

[60] Yu, X. Z. *et al.* Real-space observation of a two-dimensional skyrmion crystal. *Nature* **465**, 901–904 (2010).

[61] Brearton, R. *et al.* Deriving the skyrmion hall angle from skyrmion lattice dynamics. *Nature Communications* **12**, 2723 (2021).

[62] Grzybowski, B. A., Stone, H. A. & Whitesides, G. M. Dynamic self-assembly of magnetized, millimetre-sized

objects rotating at a liquid–air interface. *Nature* **405**, 1033–1036 (2000).

[63] Han, M. *et al.* Statistical mechanics of a chiral active fluid. *arXiv:2002.07679* (2020).

[64] Yeo, K., Lushi, E. & Vlahovska, P. M. Collective dynamics in a binary mixture of hydrodynamically coupled microrotors. *Phys. Rev. Lett.* **114**, 188301 (2015).

[65] Scholz, C., Engel, M. & Pöschel, T. Rotating robots move collectively and self-organize. *Nature Communications* **9**, 931 (2018).

[66] Goldman, A., Cox, R. & Brenner, H. Slow viscous motion of a sphere parallel to a plane wall—i motion through a quiescent fluid. *Chemical Engineering Science* **22**, 637–651 (1967).

[67] Aragones, J. L., Steimel, J. P. & Alexander-Katz, A. Elasticity-induced force reversal between active spinning particles in dense passive media. *Nat Commun* **7**, 11325 (2016). 1512.02562.

[68] While the quantity P corresponds to the power exerted by the interaction forces in purely mechanical systems, this physical interpretation does not carry over in gyroscopic or vortex crystals [33].

[69] Truesdell, C. A. The meaning of betti's reciprocal theorem. *Journal of Research of the National Bureau of Standards Section B Mathematics and Mathematical Physics* 85 (1963).

[70] Zubov, L. *Nonlinear Theory of Dislocations and Disclinations in Elastic Bodies*. Lecture Notes in Physics Monographs (Springer Berlin Heidelberg, 2008).

[71] Storm, C., Pastore, J. J., MacKintosh, F. C., Lubensky, T. C. & Janmey, P. A. Nonlinear elasticity in biological gels. *Nature* **435**, 191–194 (2005).

[72] Lubensky, T. C., Mukhopadhyay, R., Radzihovsky, L. & Xing, X. Symmetries and elasticity of nematic gels. *Phys. Rev. E* **66**, 011702 (2002).

[73] Antman, S., Truesdell, C. & Noll, W. *The Non-Linear Field Theories of Mechanics* (Springer Berlin Heidelberg, 2013).

[74] Ogden, R. W. (ed.) *Nonlinear elasticity : theory and applications*. London Mathematical Society lecture note series. (Cambridge University Press, Cambridge, U.K. ; New York, 2001).

[75] See the Supplemental Material for additional discussion, including Refs. [77–85].

[76] Landau, L. *et al.* *Theory of Elasticity*. Course of theoretical physics (Elsevier Science, 1986).

[77] Born, M. *Dynamical theory of crystal lattices*. The International series of monographs on physics (Clarendon Press, Oxford, 1954).

[78] Fruchart, M. & Vitelli, V. Symmetries and dualities in the theory of elasticity. *Phys. Rev. Lett.* **124**, 248001 (2020).

[79] Nelson, D.R. & Peliti, L. Fluctuations in membranes with crystalline and hexatic order. *J. Phys. France* **48**, 1085–1092 (1987).

[80] Anderson, J. A., Lorenz, C. D. & Travesset, A. General purpose molecular dynamics simulations fully implemented on graphics processing units. *Journal of Computational Physics* **227**, 5342–5359 (2008).

[81] Glaser, J. *et al.* Strong scaling of general-purpose molecular dynamics simulations on GPUs. *Computer Physics Communications* **192**, 97–107 (2015).

[82] Jones, J. E. On the determination of molecular fields.i. from the variation of the viscosity of a gas with temperature. *Proceedings of the Royal Society of London. Series A, Containing Papers of a Mathematical and Physical Character* **106**, 441–462 (1924).

[83] Kim, S. & Karrila, S. J. *Microhydrodynamics: principles and selected applications* (Courier Corporation, 2013).

[84] Yukawa, H. On the interaction of elementary particles. i. *Proceedings of the Physico-Mathematical Society of Japan. 3rd Series* **17**, 48–57 (1935).

[85] Yang, J. Z., Wu, X. & Li, X. A generalized irving–kirkwood formula for the calculation of stress in molecular dynamics models. *The Journal of Chemical Physics* **137**, 134104 (2012).